Optical spectroscopy of a surface at the nanometer scale: A theoretical study in real space

Christian Girard
Laboratoire de Physique Moléculaire, Université de Franche Comté, 25030 Besançon Cedex, France

Alain Dereux
Institute for Studies in Interface Sciences, Facultés Universitaire Notre-Dame de la Paix, 61, rue de Bruxelles, B-5000 Namur, Belgium

(Received 29 January 1993; revised manuscript received 7 October 1993)

The near-field optical interaction between a pointed detector and dielectric or metallic substrates can be exploited to perform nanometer-scale surface spectroscopy. This paper presents a general framework for a realistic description of the optical near field with application to local spectroscopy of metallic aggregates deposited on a transparent sample. The treatment is based on the field-susceptibility method associated with perturbation theory. The practical solution of this model by discretization in real space is obtained by a self-consistent procedure which takes all multiple-scattering effects into account. Numerical results illustrate the evolution of direct space images when scanning metallic aggregates at various frequencies. Our simulations clearly show the interest of such a local spectroscopy for morphologic studies and for the characterization of surface mesoscopic structures.

I. INTRODUCTION

A recently developed way to gather optical information on nanometer-scale structures lying on a surface is by exploiting the optical near field.[1,2] The potential of optical scanning probe techniques for optical microscopy with lateral nanometer-scale resolution has been convincingly demonstrated by several groups over the last years.[1-9] The correlation of subwavelength-resolved optical signals with other properties such as shape, polarizability, or refraction index provides new opportunities for the characterization of surfaces. In these scanning near-field optical-microscope (SNOM) experiments, the individual structures lying on the surface induce some distortion of the near field established by the self-consistent optical interaction between probe and sample. These distortions are confined around the individual structures. Experimental studies clearly indicate that such a confined field strongly varies along the surface reproducing a particular relief of the object under test. Recently, by exploiting confined fields associated with resonance phenomena, the scanning plasmon near-field microscope reached the resolution of $\lambda/200$ on silver samples.[10] In order to guide the continued development of new probes and to understand the contrast mechanism involved in near-field optics, numerous theoretical approaches and simulations have already been proposed.[11-15] Recently the material was reviewed by Van Labeke and Barchiesi.[16]

The SNOM can also operate in the spectroscopic mode.[2,17,18] For example, if a spectroscopic event occurs at a given site of the substrate, then the signal detected by the probe can be used to perform a local spectroscopy of the surface. Recently, ruby photoluminescence spectra have been monitored with such a device.[17] In a similar way, the SNOM offers an interesting opportunity for studying localized surface plasmons near a metal island film.[18] For such metallic objects the excitation frequency ω_0 becomes an important parameter. The excitation of surface plasmons causes a characteristic field enhancement compared to the incident electromagnetic wave. In this case the efficiency of the tip-sample coupling depends on the relative magnitude of the eigenfrequencies of the probe-object system with respect to the frequency ω.[19]

In this work, we will address questions raised by such confined field associated with the resonance (plasmon) effect occurring on the sample surface as a function of the incident frequency. Our study is pertinent with respect to the spectroscopic potential of the SNOM. This paper applies a general framework for a realistic description of the optical near field to the local spectroscopy of metallic nanoparticles deposited on a transparent sample. The traditional method of solving Maxwell's equations by matching boundary conditions is restricted to a few specific geometries where the vector wave equation is separable, and is not efficient for studying low-symmetry systems such as the tip-sample system used in SNOM. In order to achieve the generality required for the description of SNOM, the method used to solve Maxwell's equations should be independent of the standard algebra implied by matching boundary conditions on both the object and the detector. The field susceptibility method[20-24] associated with perturbation theory[25,26] to be applied in this paper offers these features. The paper is organized as follows. In Sec. II we define the geometry of the problem and write the self-consistent integral equation. Efficient practical solutions of this model are found by discretization in direct space.[25-27] Individual response properties of metallic particles will be described in Sec. III and simulations of local spectroscopy experiments near a monolayer of metal particles will be presented in Sec. IV. The influence of different external parameters (location of the detector, sample material properties, etc.) on the spectral resolution will also be discussed.

II. THE SELF-CONSISTENT PROBLEM

A. General

Let $\mathbf{E}_0(\mathbf{r},\omega)$ be the Fourier component of the incident field on a highly symmetrical system (for example, the perfectly planar surface that we will consider in our application). In the presence of both a localized defect and the SNOM detector (cf. Fig. 1), the general solution of the perturbed field $\mathbf{E}(\mathbf{r},\omega)$ verifies the following implicit Lippmann-Schwinger equation:[27,28]

$$\mathbf{E}(\mathbf{r},\omega)=\mathbf{E}_0(\mathbf{r},\omega)+\int\int \mathbf{S}(\mathbf{r},\mathbf{r}',\omega)\chi(\mathbf{r}',\mathbf{r}'',\omega)\mathbf{E}(\mathbf{r}'',\omega)d\mathbf{r}'d\mathbf{r}'' \ . \quad (1)$$

At this stage it is important to recall that the first term of this self-consistent equation corresponds to the field in the absence of the probe-object system. The second term then gives the modification of this electric field due to the polarization of both the probe and object. Moreover $\mathbf{S}(\mathbf{r},\mathbf{r}',\omega)$ represents the field susceptibility of the reference system (cf. Fig. 1), and $\chi(\mathbf{r}',\mathbf{r}'',\omega)$ is the linear susceptibility of the perturbation (localized defect plus probe tip). In this description, the quantity

$$\mathbf{P}(\mathbf{r}',\omega)=\int \chi(\mathbf{r}',\mathbf{r}'',\omega)\mathbf{E}(\mathbf{r}'',\omega)d\mathbf{r}'' \quad (2)$$

occurring in Eq. (1) is the self-consistent polarization density of the probe-object system which is induced by the local electric field.

An essential advantage of this description is provided by the spatial localization of the perturbation which allows to solve exactly the self-consistent Eq. (1), as will be shown in Sec. II B. Moreover, working in direct space rather than in reciprocal space, one avoids difficulties due to the poor convergence of the Fourier series involved in standard reciprocal space descriptions.

In the upper half-space ($z \geq 0$), the second-rank tensor $\mathbf{S}(\mathbf{r},\mathbf{r}',\omega)$ is the sum of two contributions:

$$\mathbf{S}(\mathbf{r},\mathbf{r}',\omega)=\mathbf{S}_0(\mathbf{r},\mathbf{r}',\omega)+\mathbf{S}_s(\mathbf{r},\mathbf{r}',\omega) \ , \quad (3)$$

where the first term represents the field propagator in vacuum. The presence of a surface at $z=0$ is described by the field susceptibility $\mathbf{S}_s(\mathbf{r},\mathbf{r}',\omega)$. In a general way this response function can be expressed in term of quantum states $|r\rangle$ of the reference system:[20]

$$\mathbf{S}_s(\mathbf{r},\mathbf{r}',\omega)=\frac{1}{\hbar}\sum_r \left\{ \frac{\mathbf{E}_s^{0r}(\mathbf{r}')\mathbf{E}_s^{r0}(\mathbf{r})}{\omega-\omega_{r0}-i\Gamma_{r0}} - \frac{\mathbf{E}_s^{0r}(\mathbf{r})\mathbf{E}_s^{r0}(\mathbf{r}')}{\omega+\omega_{r0}-i\Gamma_{r0}} \right\} . \quad (4)$$

In this expression the terms $\mathbf{E}_s^{0r}(\mathbf{r})$ represent the matrix elements of the electric-field operator of the solid surface (reference system) between the fundamental state and the rth excited state, and the coefficient Γ_{r0} are the corresponding damping parameters. The field susceptibility defined in (3) can also be built by calculating the response field of the reference system to an arbitrary fluctuating dipole lying in its neighborhood. In the particular case of a solid (dielectric or metallic) limited by a perfectly planar surface, various theoretical methods have been developed to obtain this response function. The analytical form of $\mathbf{S}(\mathbf{r},\mathbf{r}',\omega)$ depends on the nature of the surface under consideration.[20–24,29] To treat a crystallographic face of an ionic crystal, it is more convenient to use a discrete atomic representation of the solid structure.[30] When dealing with a metal, this susceptibility can be modeled from a continuous approach in order to account for the delocalized character of the free-electron response.[23] In the numerical work to be discussed in this paper, the analytical form of $\mathbf{S}(\mathbf{r},\mathbf{r}',\omega)$ can be found in Ref. 19, Eqs. (23) and (24).

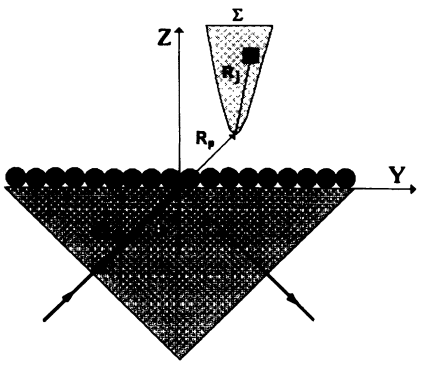

FIG. 1. Illustration of an experimental device working in total reflection [scanning tunneling optical microscope (STOM), also called the photon scanning tunneling microscope (PSTM)]. The light beam of wave vector $\mathbf{K}_0$ is totally reflected on the plane surface of a transparent medium. The object is composed of m metallic spheres deposited on the surface ($z=0$). The vector $\mathbf{R}_P=(X_P,Y_P,Z_P)$ defines the detector apex position, and $\mathbf{R}_j$ characterizes the location of a given volume element inside the tip.

B. Effective field inside the probe-sample system

In SNOM experimental setups, the main element is the tip of a dielectric stylus. Actually the current trend is the use of monomode fibers whose cone-shaped tip is obtained by different techniques such as chemical etching or pulling-heating processes. In the present application the optical probe will be treated as a continuous medium of refraction index n_{pr}. In this subsection we consider the problem of such a pointed dielectric stylus facing a set of m spherical nanoparticles deposited upon a plane dielectric surface (cf. Fig. 1). There are various ways of describing the response properties of such metallic objects. Maxwell's equations can be solved by applying standard boundary conditions to the surface of the metallic aggregate. This approach leads us to introduce a bulk dielectric constant of the metal. A different method based on the multipolar expansion of each metallic particles can also be adopted. This last approach, which appears to be more adequate to account for nonlocal effects, will be developed in this section.

In experimental devices, the probe and sample always remain well-separated systems during a scan. Consequently the electric susceptibility $\chi(\mathbf{r},\mathbf{r}',\omega)$ describing the linear-response properties of the perturbation can be

written as the sum of two contributions associated with the probe and the object, respectively:

$$\chi(\mathbf{r},\mathbf{r}',\omega)=\chi_{\mathrm{pr}}(\mathbf{r},\mathbf{r}',\omega)+\chi_{\mathrm{ob}}(\mathbf{r},\mathbf{r}',\omega) \ . \tag{5}$$

The spheres forming the monolayer lie at a constant distance Z_0 from the surface. In the first approximation we consider that the quantum electronic states of the spheres composing the object are weakly perturbed. We can then write χ_{ob} as a sum of individual susceptibilities:

$$\chi_{\mathrm{ob}}(\mathbf{r},\mathbf{r}',\omega)=\sum_{i=1}^{m}\chi_i(\mathbf{r},\mathbf{r}',\omega) \ , \tag{6}$$

where the subscript i is needed to define the location of a sphere in a plane parallel to the surface. For metallic particles of subwavelength size, the nonlocal susceptibility χ_i can be expanded as a series of dynamical multipolar polarizabilities:[31]

$$\chi_i(\mathbf{r},\mathbf{r}',\omega)=\alpha^{(1)}(\omega)\delta(\mathbf{r}-\mathbf{r}_i)\delta(\mathbf{r}'-\mathbf{r}_i)+\tfrac{1}{9}\alpha^{(2)}(\omega)[2]\nabla_{\mathbf{r}}\nabla_{\mathbf{r}'}\delta(\mathbf{r}-\mathbf{r}_i)\delta(\mathbf{r}'-\mathbf{r}_i)+\cdots$$
$$+\frac{1}{[(2p-1)!!]^2}\alpha^{(p)}(\omega)[2p-2]\nabla_{\mathbf{r}}^{(p-1)}\nabla_{\mathbf{r}}^{(p-1)}\delta(\mathbf{r}-\mathbf{r}_i)\delta(\mathbf{r}'-\mathbf{r}_i) \ , \tag{7}$$

where $\nabla_{\mathbf{r}}$ is the gradient operator, $\mathbf{r}_i$ represents the position vectors of the spheres, and $\alpha^{(p)}(\omega)$ defines their multipolar polarizabilities. Moreover, the symbol $[p]$ indicates a total contraction of two pth-order tensors. In the case of noble-metal particles, the charge-density susceptibility approach provides a good framework to describe the response functions $\alpha^{(p)}$ in the optical range.

The integral equation (1) can be expressed in terms of effective fields and field gradients existing at each site occupied by the spheres

$$\mathbf{E}(\mathbf{r},\omega)=\mathbf{E}_0(\mathbf{r},\omega)+\mathcal{E}_{\mathrm{pr}}(\mathbf{r},\omega)+\mathcal{E}_{\mathrm{ob}}(\mathbf{r},\omega) \ . \tag{8}$$

In this last equation, the second term is proportional to the perturbation induced by the detector extremity

$$\mathcal{E}_{\mathrm{pr}}(\mathbf{r},\omega)=\int\int_{\mathrm{pr}}\mathbf{S}(\mathbf{r},\mathbf{r}',\omega)\chi_{\mathrm{pr}}(\mathbf{r}',\mathbf{r}'',\omega)\mathbf{E}(\mathbf{r}'',\omega)d\mathbf{r}'d\mathbf{r}'' \ . \tag{9}$$

The response of this dielectric stylus is assumed to be local. It is then possible to express $\mathcal{E}_{\mathrm{pr}}$ from the refraction index n_{pr} of the detector:[32]

$$\mathcal{E}_{\mathrm{pr}}(\mathbf{r},\omega)=\frac{n_{\mathrm{pr}}^2(\omega)-1}{4\pi}\int_{\mathrm{pr}}\mathbf{S}(\mathbf{r},\mathbf{r}',\omega)\mathbf{E}(\mathbf{r}',\omega)d\mathbf{r}' \ . \tag{10}$$

This last integral can be calculated by discretization in Cartesian space, and optimized by using a tridimensional Gauss method.[25] This leads to

$$\mathcal{E}_{\mathrm{pr}}(\mathbf{r},\omega)=\frac{n_{\mathrm{pr}}^2(\omega)-1}{4\pi}\sum_{j=1}^{n}W_j\mathbf{S}(\mathbf{r},\mathbf{r}_j,\omega)\mathbf{E}(\mathbf{r}_j,\omega) \ , \tag{11}$$

where W_j represents the weight of the jth discretized element in the tip apex.

By taking (5), (6), and (7) into account, the term proportional to the perturbation induced by the metal particles in Eq. (7) is given by

$$\mathcal{E}_{\mathrm{ob}}(\mathbf{r},\omega)=\sum_{p}\sum_{i=1}^{m}\frac{1}{[(2p-1)!!]^2}\{\nabla_{\mathbf{r}'}^{(p-1)}\mathbf{S}(\mathbf{r},\mathbf{r}',\omega)\}_{\mathbf{r}'=\mathbf{r}_i}[p]\alpha^{(p)}[p]\mathbf{F}^{(p)}(\mathbf{r}_i,\omega) \ , \tag{12}$$

where the tensors $\mathbf{F}^{(p)}$ describe the successive field gradients experienced by each metal particle

$$\mathbf{F}^{(p)}(\mathbf{r}_i,\omega)=\{\nabla_{\mathbf{r}}^{(p-1)}[\mathbf{E}_0(\mathbf{r},\omega)+\mathcal{E}_{\mathrm{pr}}(\mathbf{r},\omega)+\mathcal{E}_{\mathrm{ob}}(\mathbf{r},\omega)]\}_{\mathbf{r}=\mathbf{r}_i} \ . \tag{13}$$

For metallic particles of small size, the multipolar contributions higher than the dipolar one in Eq. (12) will be neglected, resulting in a single summation for the spheres' positions. In this approximation the number of discretization points is then identical to the number of metallic particles. Equation (12) reduces to

$$\mathcal{E}_{\mathrm{ob}}(\mathbf{r},\omega)=\sum_{i=1}^{m}\mathbf{S}(\mathbf{r},\mathbf{r}_i,\omega)\alpha^{(1)}(\omega)\mathbf{E}(\mathbf{r}_i,\omega) \ . \tag{14}$$

Let us note that a more refined calculation of both local field and local-field gradients at each site occupied by the metallic particles would require us to go beyond the dipolar approximation. In fact, the truncation of the multipolar expansion depends on the length scale over which the local field varies inside the probe sample system, and the dipolar approximation used to treat the response of the spheres must be considered as a first step toward an all-orders calculation. This approximation avoids the computational difficulties involved in a complete multipolar self-consistent calculation, and nevertheless gives a reasonable description of the optical spectroscopy of a surface at the nanometer scale. In this context an essential strength of the present treatment is the spatial localization of the defect, which allows us to solve the self-

consistent equation (8) exactly. Indeed, both indices n and m remain finite, so that the resulting matrix equation can be solved by standard linear algebra procedures

$$\mathbf{E}(\mathbf{r}_k,\omega)=\mathbf{E}_0(\mathbf{r}_k,\omega)+\sum_{l=1}^{n+m}\mathbf{S}(\mathbf{r}_k,\mathbf{r}_l,\omega)\alpha_l(\omega)\mathbf{E}(\mathbf{r}_l,\omega)\ , \tag{15}$$

where the quantity $\alpha_l(\omega)$ has the dimension of a dynamical polarizability and changes its value according to the index l:

$$\alpha_l(\omega)=\alpha^{(1)}(\omega)\quad \text{if } (1\le l\le m) \tag{16}$$

and

$$\alpha_l(\omega)=\left\{\frac{n_{\rm pr}^2(\omega)-1}{4\pi}\right\}W_l\quad \text{if } (m+1\le l\le n+m)\ . \tag{17}$$

We note that the procedure avoids matching boundary conditions. The latter are in fact implicitly guaranteed by the self-consistency of the original integral equations (1) and (15). The only approximation of the technique lies in the density of the discretization grid, which is arbitrarily adjustable.

C. Signal detected by the tip

The conversion process of evanescent waves in the immediate proximity of the object into homogeneous waves propagating in the detector can be described from the above results. In fact, knowledge of the effective-field distribution inside the perturbation is sufficient to describe the far-field $\mathbf{E}_{\rm far}$ crossing a surface located in the wave zone of the dielectric stylus (cf. Fig. 1):

$$\mathbf{E}_{\rm far}(\mathbf{R}_p+\mathbf{r}_0,\omega)=\sum_{k=1}^{n+m}\mathbf{S}(\mathbf{R}_p+\mathbf{r}_0,\mathbf{r}_k,\omega)\alpha_k(\omega)\mathbf{E}(\mathbf{r}_k,\omega)\ , \tag{18}$$

where $\mathbf{R}_p$ defines the location of the tip apex with respect to an absolute frame, and the vector $\mathbf{r}_0$ represents the position of a point of the Σ surface with respect to the apex of the detector. In fact, Eq. (18) means that the solution inside the localized perturbation does not depend on the solution outside the perturbation (object plus probe). Thus, by using an asymptotic form of the propagator $\mathbf{S}$ in the far-field range, it is possible to describe regions far from the perturbation. Finally, numerical integration of the Poynting vector associated with $\mathbf{E}_{\rm far}(\mathbf{R}_p+\mathbf{r}_0,\omega)$ on the surface of the cross section Σ of the probe leads to the energy flux across that section and hence the detected intensity $I(\mathbf{R}_p,\omega)$, which is the relevant observable in current SNOM experiments.

III. INDIVIDUAL RESPONSE PROPERTIES OF METALLIC NANOPARTICLES

The study of the optical linear-response properties of small metallic aggregates has been extensively investigated for the last 20 years.[33–39] In the case of metal spheres embedded in a transparent dielectric, the interface between the two materials introduces a surface-plasmon resonance whose frequency depends on the optical properties of the metal and on the surrounding dielectric constant. Recently, a theoretical approach based on the charge-density susceptibility formalism has been applied to a spherical jellium.[39] In our work the main aspects of the optical properties of the particles are introduced by generalizing the method of Newns[40] to an electron gas confined in a spherical well. From this model the multipolar polarizabilities $\alpha^{(p)}$ of noble-metal particles can be described by introducing the interband electronic contributions of the metal from standard experimental data.[41] In fact, this problem can be solved by including all terms for which $p>1$ in the treatment presented in Ref. 39. For first- and second-order polarizabilities, such a procedure leads to

$$\alpha^{(1)}(\omega)=a^3\left\{\frac{1-F_1(a,\omega)/a}{2F_1(a,\omega)/a+1}\right\} \tag{19}$$

and

$$\alpha^{(2)}(\omega)=\tfrac{3}{2}a^5\left\{\frac{1-2F_2(a,\omega)/a}{3F_2(a,\omega)/a+1}\right\}\ , \tag{20}$$

with

$$F_p(a,\omega)=\frac{2}{a}\sum_k\left\{\frac{j_p^2(ka)k^{-2}}{j_p^2(ka)-j_{p+1}(ka)j_{p-1}(ka)}\right\}\epsilon_m^{-1}(\omega,k)\ , \tag{21}$$

where a is the radius of the metallic sphere, j_p is the pth spherical Bessel function, and $\epsilon_m(\omega,k)$ represents the nonlocal bulk dielectric constant of the metal.

IV. LOCAL SPECTROSCOPY OF NOBLE-METAL PARTICLES DEPOSITED ON A TRANSPARENT SAMPLE

The two relations (15) and (18) defined in previous sections are general, since they account for the real profile of the tip apex and they include, through $\alpha^{(1)}(\omega)$, the dynamical properties of the metallic particles forming the object. From these equations it is possible to calculate the signal $I(\mathbf{R}_p,\omega)$ and to simulate, for a fixed location of the detector, a local spectroscopy experiment. For this study, the dipolar dynamical polarizability of the metallic particles will be described from Eq. (19) by including spatial dispersion effects through a hydrodynamic dielectric constant.[35] Furthermore, the discussion will be presented in the internal total reflection (STOM/PSTM, where PSTM is the photon scanning tunneling microscope) configuration described in Fig. 1.[3,4,6,9]

For metallic objects, the excitation frequency ω of the incident field becomes an important parameter. In the region above the surface of the sample, where the evanescent field is sensed, it is possible to restore the spectroscopic characteristics of nanometric-sized particles by varying the external frequency. Surface particles have

often been used in enhancement studies.[42] They are easily produced and can generate a strong local field. In particular, silver and gold island films have been extensively studied in the past because of their unusual optical properties.[43] Such objects appear to be interesting systems to test local spectroscopy properties in the optical range.

The influence of ω on the magnitude of the detected intensity is numerically studied in Figs. 2, 3, and 5, where we present the frequency-dependent intensity $I(\mathbf{R}_p,\omega)$ for particular positions $\mathbf{R}_p$ of the detector. All results are presented in p-polarized illumination. The incident angle of the light beam is $\theta_0=60°$, and the incident wave vector $\mathbf{K}_0$ is located in the plane (YOZ).

Figure 2 describes the evolution of the spectrum recorded near a single metallic particle for different lateral positions of the tip apex. The approach distance (Z_p in Fig. 1) between the detector edge and the plane support is kept constant. A spatially extended probe tip (20-nm curvature at its extremity, 70-nm height), discretized by 36 cells in a closed-packed arrangement, was considered in all our calculations. As expected, the localized plasmon peak collapses when the detector moves away. For example in the case of gold [Fig. 2(a)], beyond a distance of 50 nm the plasmon resonance becomes undetectable. One observes in the successive curves of Fig.

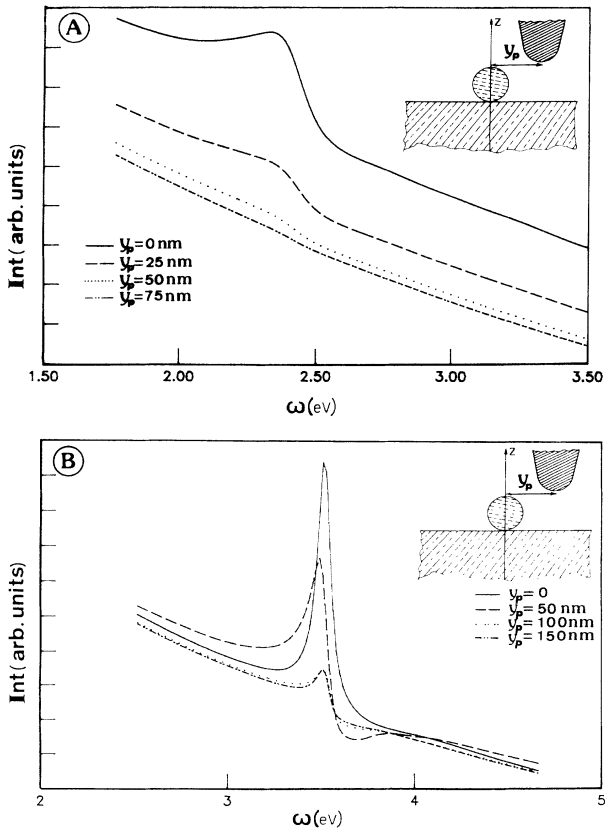

FIG. 2. Study of the behavior of the detected intensity as a function of the incident field frequency. The object is a single metallic particle of 15-nm radius located at the origin of the absolute frame. The tip-surface distance is maintained constant ($Z_P=32$ nm). (a) Gold sphere. (b) Silver sphere.

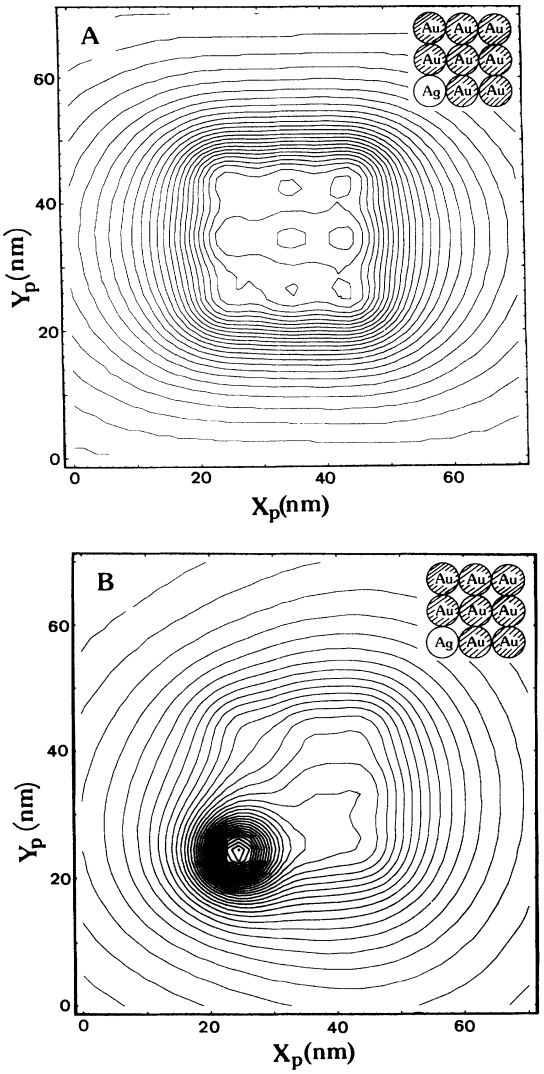

FIG. 3. Isointensity curves detected above an aggregate composed of nine noble metal particles of different nature (the sphere located at the corner of the pattern is in silver, the others are in gold). The calculation is performed in a plane parallel to the surface ($Z_P=11$ nm). The 10-nm-diameter spheres are organized on the surface as a square lattice and the scanned area is (70×70) nm^2. (a) The frequency ω of the incident field is equal to 2 eV. (b) $\omega=3.34$ eV.

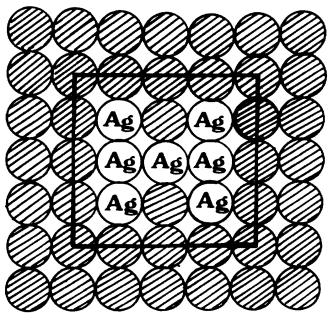

FIG. 4. Square geometry of the layered metallic nanoparticles used in the calculations of Fig. 5. The gold spheres of 10 nm diameter are schematized by large shaded circles. The square limited by solid lines represents the scanned area.

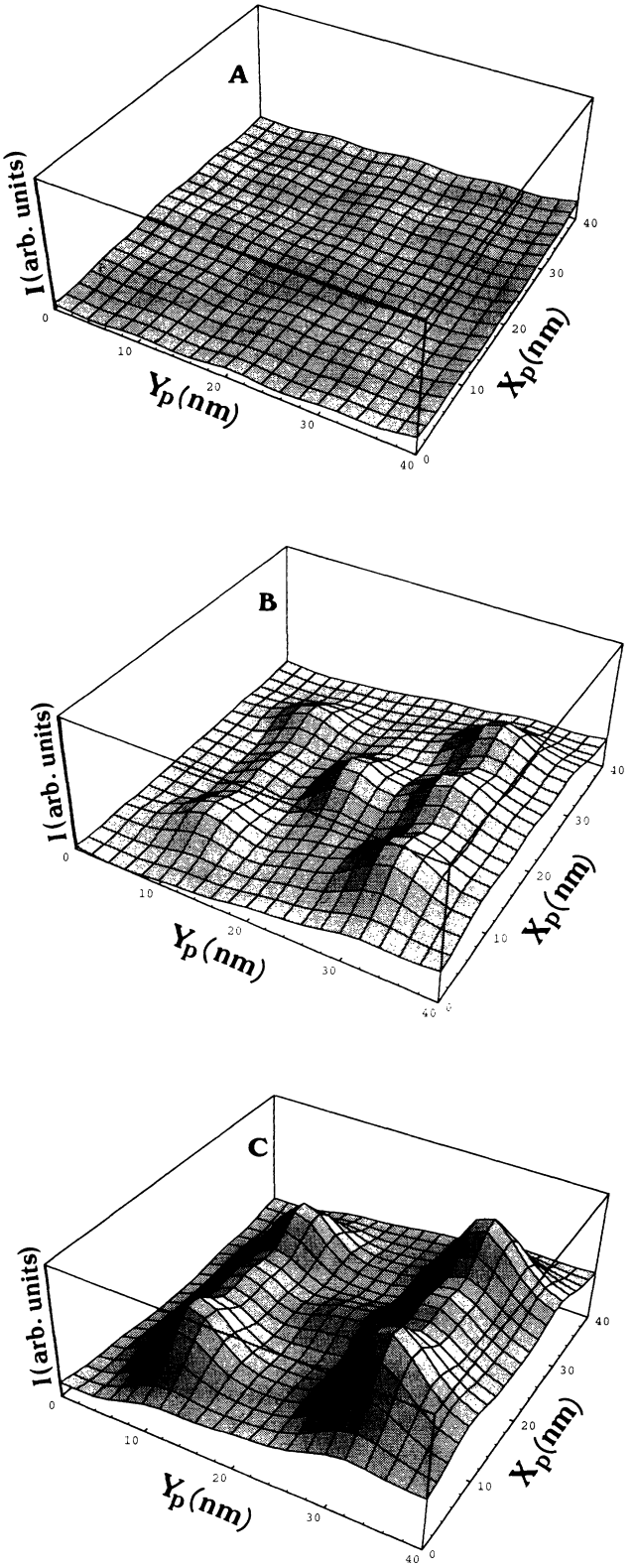

FIG. 5. A sequence of NFO images calculated in constant distance mode ($Z_P = 12$ nm). The object is described in Fig. 4. The curvature tip end and the scanned area are 15 nm and (40×40) nm^2, respectively. The silver spheres appear to be well resolved when the incident frequency reaches 3.2 eV. (a) $\omega = 2$ eV. (b) $\omega = 3.1$ eV. (c) $\omega = 3.3$ eV.

2 that a slight redshift of the plasmon resonance occurs when Y_p decreases. The shift is due to the presence of the detector approaching the metal particles. It is similar to the shift observed when noble-metal particles are embedded in a transparent dielectric medium.[33]

Figure 3 presents an ensemble of isointensity curves detected above an aggregate composed of nine noble-metal particles. The sphere located at the corner of the pattern is made of silver, and the others of gold. The calculation of these isointensity curves is performed in a plane parallel to the dielectric support ($Z_p = 11$ nm), and the 10-nm-diameter spheres are organized on the surface at the nodes of a square lattice. A surface of 70×70 nm^2 is scanned around and above the aggregate. One remarks that the density of the isointensity curves increases in the direction (OY) of the light beam propagation. Moreover, by working far from the localized plasmon resonance of the silver sphere [See Fig. 3(a)], the intensity distribution detected by the probe tip retains the square symmetry of the aggregate. This result is consistent with the magnitude of the individual polarizabilities of gold and silver spheres in this frequency range. Now when the external frequency ω reaches the plasmon frequency of the silver spheres, the electric field is enhanced at the immediate proximity of this particle and induces a strong distortion in the intensity distribution. It is then possible to discriminate between different kinds of metallic particles.

Figure 5 illustrates the behavior of the constant distance image of the monolayer of metallic particles described in Fig. 4. In this application, the aggregate consists of a set of seven 10-nm-diameter silver particles surrounded by gold spheres of the same size. The silver spheres are organized on the substrate like a letter **H**, and the scanned area is centered around this pattern as illustrate in Fig. 4. It may be seen in Fig. [5(a)] that around 2 eV the image corrugations are weak. In contrast, when the frequency increases to reach the localized resonance of the set of silver particles [see Fig. 5(b) and 5c)] the shape of the images is dramatically changed. In fact, around this resonant model [Fig. 5(c)], the form of the letter H may be recognized, though with some distortion due to depolarization effects occurring at the center of the pattern.

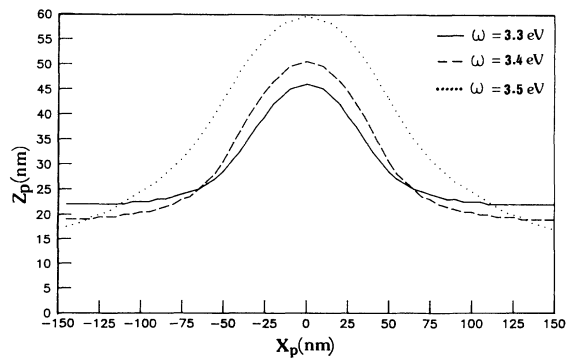

FIG. 6. Frequency-dependent study of the deflection experienced by the dielectric probe tip above a silver particle 15 nm in radius.

In many experimental studies, near-field optical (NFO) images are recorded by keeping the detected intensity at a constant level with a feedback mechanism.[3,4,6,7,9,10] Thus, when the tip is displaced along the surface being tested, it follows the contour of the object, and the images are obtained by measuring the deflection of the detector. A simulation of this operating mode is given in Fig. 6, where we have calculated the trajectory of the tip apex above a single silver particle 15 nm in radius. As expected, the amplitude of the deflection above the sphere depends on the incident-field frequency. Near the plasmon resonance this deflection reaches 35 nm and reveals the presence of a strong enhanced electric near field.

V. CONCLUSION

We have theoretically analyzed, in systems of experimental interest, the possibility of performing local spectroscopy for a surface with a near-field optical microscopic working in the STOM/PSTM configuration. Starting from a Lippmann-Schwinger version of Maxwell's equations, we have studied the near-field behavior of metallic objects at close proximity as the external frequency is varied in the optical range. The discretization procedure in direct space used to solve this implicit integral equation appears to be well suited for dealing with realistic situations, since it is independent of the boundary shapes and accounts for any kind of dielectric function profile. Numerical simulations have been performed by discretizing the apex of a dielectric stylus. For such a detector, the interaction between the detection device and the object weakly perturbs the spectral characteristics of the system to be analyzed. The authors hope that the simulations presented in this paper stimulate experimental development toward scanning optical spectroscopy. If such an experiment becomes possible, it should be kept in mind that the uncertainty about the nanoparticles susceptibilities might induce some quantitative deviations from our results; in particular, the resonance peaks could turn out to be somewhat shifted. Nevertheless, the aim of our simulations is not the exact determination of such peak values but rather to show the interest of such a method for morphologic studies and for the characterization of structures in the mesoscopic range.

ACKNOWLEDGMENTS

The authors express their sincere thanks to Dr. D. Courjon, Dr. D. W. Pohl, and Professor J. P. Vigneron for a number of stimulating and interesting discussions. One of us (A.D.), acknowledges the Walloon Ministry for Research and Technology (Brussels) for financial support.

[1]D. W. Pohl, Adv. Opt. Electron. Microsc. **12**, 243 (1991), and references therein.
[2]E. Betzig, J. K. Trautman, T. D. Harris, J. S. Weiner, and R. L. Kostelak, Science **251**, 1468 (1991), and references therein.
[3]R. Reddick, R. J. Warmack, and T. J. Ferrell, Phys. Rev. B **39**, 767 (1989).
[4]D. Courjon, K. Sarayeddine, and M. Spajer, Opt. Commun. **71**, 23 (1989).
[5]J. A. Cline, H. Barshatzky, and M. Isaacson, Ultramicroscopy **38**, 299 (1991).
[6]N. F. Van Hulst, F. B. Segering, and B. Bolger, Opt. Commun. **87**, 212 (1992).
[7]K. Lieberman and A. Lewis, Ultramicroscopy **42-44**, 399 (1991).
[8]T. L. Ferrell, S. L. Sharp, and R. J. Warmack, Ultramicroscopy **42-44**, 408 (1991).
[9]F. de Fornel, L. Salomon, P. Adam, E. Bourillot, J. P. Goudonnet, and M. Neviere, Ultramicroscopy **42-44**, 422 (1992).
[10]M. Specht, J. D. Pedarnig, W. M. Heckl, and T. W. Hansch, Phys. Rev. Lett. **68**, 496 (1992).
[11]C. Girard and D. Courjon, Phys. Rev. B **42**, 9340 (1990).
[12]A. Roberts, J. Appl. Phys. **70**, 4045 (1991).
[13]D. Van Labeke and D. Barchiesi, J. Opt. Soc. Am. A **9**, 732 (1992).
[14]O. Keller, M. Xiao, and S. Bozhevolnyi, Surf. Sci. **280**, 217 (1993).
[15]S. Berntsen, E. Bozhevolnaya, and S. Bozhevolnyi, J. Opt. Soc. Am. A **10**, 878 (1993).
[16]D. Van Labeke and D. Barchiesi, in *Near Field Optics,* Vol. 242 of *NATO Advanced Study Institute Series E: Applied Sciences,* edited by D. Pohl and D. Courjon (Kluwer, Dordrecht, 1993).
[17]M. A. Paesler, P. J. Moyer, C. J. Jahncke, C. E. Johnson, R. C. Reddick, R. J. Warmack, and T. L. Ferrell, Phys. Rev. B **42**, 6750 (1990).
[18]H. Bielefeldt, B. Hecht, S. Herminghaus, O. Marti, and J. Mlynek, in *Near Field Optics* (Ref. 16).
[19]C. Girard and X. Bouju, J. Chem. Phys. **95**, 2056 (1991).
[20]A. D. McLachlan, Mol. Phys. **7**, 381 (1964).
[21]G. S. Agarwal, Phys. Rev. A **11**, 230 (1975).
[22]H. Metiu, J. Chem. Phys. **76**, 1765 (1982).
[23]H. Metiu, Prog. Surf. Sci. **17**, 153 (1984).
[24]H. Metiu and P. Das, Ann. Rev. Phys. Chem. **35**, 507 (1984).
[25]A. Dereux, Ph.D. thesis, Faculté Universitaire N. D. de la Paix, NAMUR, Belgium, 1991.
[26]A. Dereux, J. P. Vigneron, Ph. Lambin, and A. A. Lucas, Physica B **175**, 65 (1991).
[27]A. D. Yaghjian, Proc. IEEE **68**, 248 (1980).
[28]E. N. Economou, *Green's Functions in Quantum Physics,* 2nd ed. (Springer, Berlin, 1983).
[29]A. M. Marvin and F. Toigo, Phys. Rev. A **25**, 782 (1982).
[30]C. Girard and C. Girardet, J. Chem. Phys. **86**, 6581 (1987).
[31]A. D. Buckingham, Adv. Chem. Phys. **12**, 107 (1967).
[32]C. G. Bohren and D. R. Huffman, in *Absorption and Scattering of Light by Small Particles,* edited by A. D. Boardman (Wiley, New York, 1983).
[33]L. Genzel, T. P. Martin, and U. Kreibig, Z. Phys. B **21**, 339 (1975).
[34]A. Kawabata and R. Kubo, J. Phys. Soc. Jpn. **21**, 1765 (1966).
[35]B. B. Dasgupta and R. Fuchs, Phys. Rev. B **24**, 554 (1981).
[36]E. Zaremba and B. N. J. Persson, Phys. Rev. B **35**, 596 (1987).
[37]W. Ekardt, Phys. Rev. B **34**, 526 (1986).
[38]G. D. Mahan and K. R. Subbaswamy, in *Local Density Theory of Polarizability,* edited by G. D. Mahan (Plenum, New York,

1990).
[39]C. Girard and F. Hache, Chem. Phys. **118**, 249 (1987).
[40]D. M. Newns, Phys. Rev. B **1**, 3304 (1970).
[41]P. B. Johnson and R. Christy, Phys. Rev. B **6**, 4370 (1972).
[42]M. Meier, A. Wokaun, and P. F. Liao, J. Opt. Soc. Am. B **2**, 931 (1985).
[43]T. Yamaguchi, S. Yoshida, and A. Kinbara, J. Opt. Soc. Am. **64**, 1563 (1974).

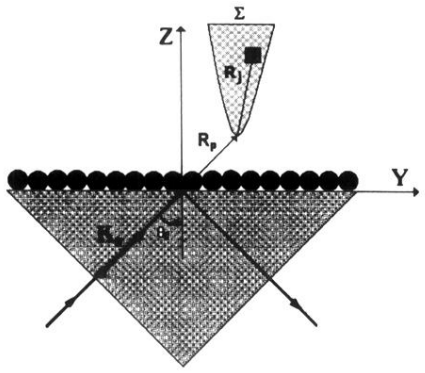

FIG. 1. Illustration of an experimental device working in total reflection [scanning tunneling optical microscope (STOM), also called the photon scanning tunneling microscope (PSTM)]. The light beam of wave vector $\mathbf{K}_0$ is totally reflected on the plane surface of a transparent medium. The object is composed of m metallic spheres deposited on the surface ($z=0$). The vector $\mathbf{R}_P=(\mathbf{X}_P,\mathbf{Y}_P,\mathbf{Z}_P)$ defines the detector apex position, and $\mathbf{R}_j$ characterizes the location of a given volume element inside the tip.

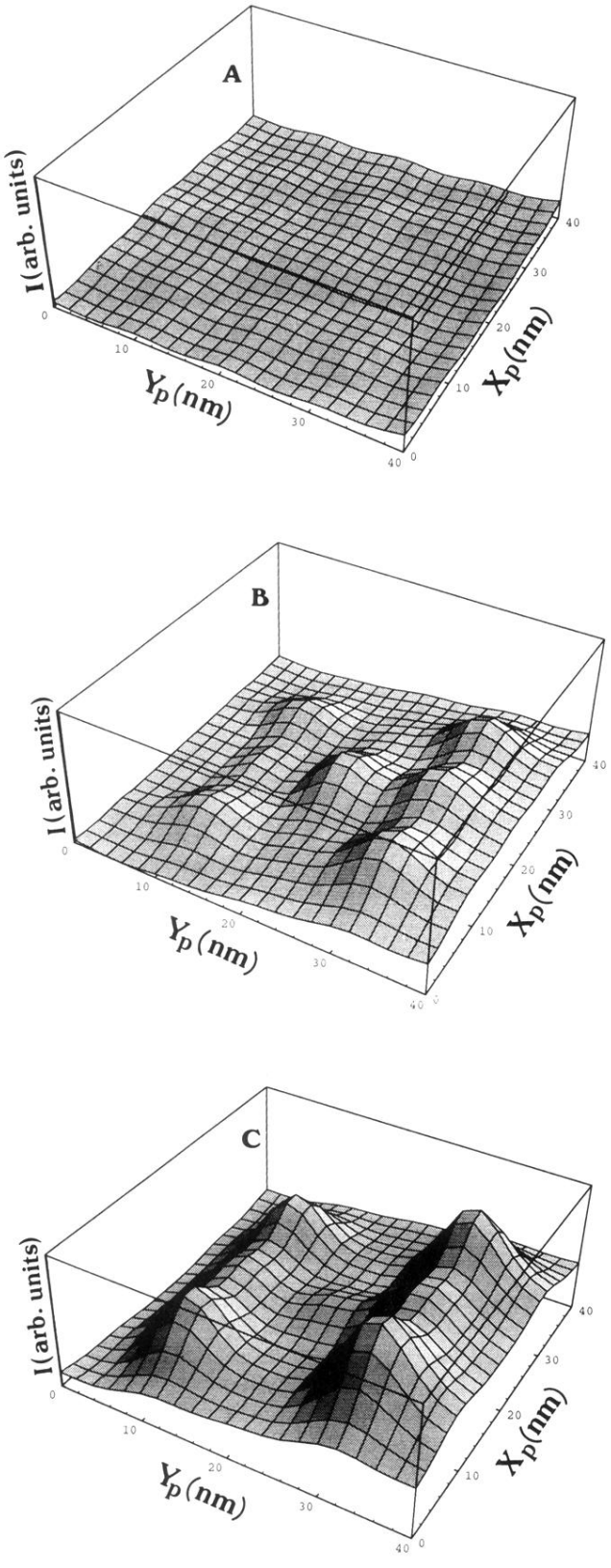

FIG. 5. A sequence of NFO images calculated in constant distance mode ($Z_P = 12$ nm). The object is described in Fig. 4. The curvature tip end and the scanned area are 15 nm and (40×40) nm^2, respectively. The silver spheres appear to be well resolved when the incident frequency reaches 3.2 eV. (a) $\omega = 2$ eV. (b) $\omega = 3.1$ eV. (c) $\omega = 3.3$ eV.